The Pressure Dependence of the Eutectic Temperature for Mixtures of Sodium Sulfate and Water

A. J. Dougherty[a,*], J. A. Avidon[a], D. L. Hogenboom[a], J. S. Kargel[b], D. K. Morris[a,1]

[a]*Department of Physics, Lafayette College, Easton, Pennsylvania, USA*
[b]*Department of Hydrology and Water Resources, University of Arizona, Tucson, Arizona, USA*

Abstract

We report the first crystal images and measurements of the eutectic temperature of sodium sulfate hydrates in water at pressures up to 375 MPa using a volumetric cell with sapphire windows. In the Ice-Ih regime we find that adding the salt causes only a modest depression in the melting temperature. In the Ice-III regime, we find evidence of two different states with different transition temperatures. All of these transitions are accompanied by significant volume changes.

Keywords: Ices, Europa, Cosmochemistry

1. Introduction

Jupiter's moon Europa is a complex world with a rich geologic history (Prockter et al., 2010). Untangling that history will involve developing a deeper understanding of how the icy surface interacts with any underlying ocean (Nimmo and Pappalardo, 2016; Neveu et al., 2017). The types and abundances of different impurities in that ocean can have significant implications for the thermodynamic, chemical and mechanical properties of that icy shell (Durham et al., 2005; McCarthy et al., 2006).

*Corresponding author.
Email address: doughera@lafayette.edu (A. J. Dougherty)
[1]Current address: Division of Geological and Planetary Sciences, California Institute of Technology, Pasadena, CA, USA

Reports of possible plumes on Europa (Roth et al., 2014; Sparks et al., 2017), as well as the overall relatively young age of much of the surface point to ongoing active processes. The chaos terrain on the leading hemisphere may be indicative of a convecting subsurface ocean interacting with the surface (Schmidt et al., 2011; Soderlund et al., 2014). The analysis in Prockter et al. (2017) of the dark and gray areas in the "pull-apart" bands suggests that the dark bands are younger and are more likely to have a significant impurity component. One possible interpretation of all these results is that there is significant interaction, and perhaps even interchange of material, between the subsurface ocean and the surface (Prockter et al., 2017; McCord et al., 2010).

Evidence for the nature of the impurities comes from the near-infrared reflectance spectra obtained from the Galileo mission for the low albedo regions on Europa's surface (Carlson et al., 1996; McCord et al., 1998, 1999). These have typically been interpreted as indicating the presence of various hydrated compounds, possibly including hydrated salts of magnesium sulfate and sodium sulfate (Dalton et al., 2005; Orlando et al., 2005; Shirley et al., 2010) as well as sulfuric acid hydrates (Shirley et al., 2010; Carlson et al., 2005). The low albedo regions may contain geologically young material, including possible cryovolcanic flows (Shirley et al., 2010). Spatially-resolved re-analysis of the NIMS spectra suggested that sulfates are preferentially located in the low albedo regions near the center of ridges (McCord et al., 2010), though other observations (Fischer et al., 2015; Ligier et al., 2016) do not show evidence of mirabilite.

Chondrite-based chemical models for the formation and evolution of Europa also suggest the importance of hydrated salts in Europa's crust (Kargel et al., 2000; Spaun and Head, 2001), though other models do suggest that the sulfate content could be considerably lower (McKinnon and Zolensky, 2003; Zolotov et al., 2006).

Analysis of sulfate compounds is complicated by interactions of the surface with Io. The radiolytic sulfur cycle is an important source of sulfur on the trailing surface of Europa (Carlson et al., 2005). An analysis of the infrared spectra across the 180° meridian suggests that the sulfate compounds are present on both hemispheres, and hence may be at least partly endogenous (Shirley et al., 2010). However, recent Earth-based observations using the Keck II telescope found magnesium sulfate concentrations primarily on the trailing hemisphere, indicating they likely came primarily from Io (Brown and Hand, 2013). Similarly, results from the New Horizons probe (Grundy

et al., 2007) suggest that the highest concentration of sulfates is on the trailing side, again consistent with an external source.

More recent observations with the Hubble Space Telescope, incorporating visible wavelengths, suggest that sulfates are primarily located on the trailing hemisphere (Trumbo et al., 2019). By contrast, the non-ice regions on the leading hemisphere are more likely dominated by sodium chloride.

An additional complication in interpreting the spectra is that compounds on the surface of Europa are subject to significant radiation damage. The work of Hand and Carlson (2015) suggests that the reddish color of the non-icy portions of the surface may be due to primarily NaCl.

Although these surface measurements show that sodium chloride is likely an important component of the non-ice regions of Europa's surface, inferring the composition of the subsurface ocean is more complex. Studies of natural analogs at hypersaline springs (Fox-Powell et al., 2019) suggest that sulfate-rich salt mixtures could have a spectral signature similar to that observed on Europa, and that details of the precipitation process mean that the observed surface composition might not provide a strong constraint on the underlying brine composition. Similarly, the modeling in Vance et al. (2019) suggests that the fractionization of brines within the ice shell may affect the transport of material and lead to differences between surface and bulk composition.

Accordingly, a more complete understanding of the complex interactions of an icy shell with a subsurface ocean will benefit from many approaches, including additional observations, modeling, analog studies, and laboratory data.

Beyond Europa, sulfate compounds have also been found on Mars (Vaniman et al., 2004; Feldman et al., 2004; Fialips et al., 2005), and are likely widespread on the surface (Szynkiewicz et al., 2014), and perhaps on the subsurface as well (Wang et al., 2013).

There are also terrestrial applications. The large volume changes associated with phase transitions in the sodium sulfate system make it an important compound used for the accelerated stress testing of concrete and other porous materials (Flatt, 2002; McMahon et al., 1992; Scherer, 2004; Haynes, 2005; Rijniers et al., 2005; Flatt et al., 2014).

In all these applications, knowledge of the thermophysical properties of the materials involved is essential for adequate modeling of the relevant phenomena.

In this paper, we present new data for the pressure dependence of the eutectic temperature for sodium sulfate in aqueous solution for pressures up

to 375 MPa. We use optical images to confirm most of the phase transitions observed. These data complement the previous work of Tanaka et al. (1992), who measured the peritectic and liquidus temperatures for the same system.

2. Experimental Method

The technique and apparatus were similar to those described in previous papers for $MgSO_4$, ammonia-water, and methanol-water mixtures (Hogenboom et al., 1995, 1997; Dougherty et al., 2018).

Approximately 1 mL of sample is loaded into a pressure cell that is placed in a copper container and immersed in an insulated, temperature-controlled ethanol/water bath. The pressure cell is adapted from the one used in Hogenboom et al. (1997), and modified to allow optical access to the sample, to aid in identifying the crystal phases. This cell is made from a 316 stainless steel block with four ports, known as a cross (High Pressure Equipment Company #60-HF6). Two opposing ports contain replaceable plugs that have sapphire windows sealed in them with epoxy. The third port contains a plug in which a silicon diode thermometer is installed. The fourth port connects the cell to the pressure system.

The sample in the pressure cell is separated from the ethylene glycol pump fluid by a vertical U-tube filled with mercury. A steel capillary tube of constant cross section forms one arm of the U-tube. A small Alnico magnet is placed in the capillary on the interface between the pump fluid and the mercury. The height of the magnet is measured by a transducer. Changes in the transducer voltage are approximately proportional to changes in sample volume. Small systematic departures from this relationship are due to imperfections in the capillary and expansion of the capillary cross-section at high pressures. Since the data runs were made at approximately constant pressure, the latter was negligible unless comparisons were made from one run to another, and even then, the expansion of the heavy-wall stainless steel tubing due to pressure was extremely small. The capillary is housed in an insulated box maintained at room temperature so thermal expansion is not a factor. As long as the sample is mostly liquid, this system allows simultaneous measurements of temperature, pressure, and volume of the sample.

The imaging system consists of a lamp that shines light through an infrared filter and optical fiber that directs the beam horizontally through the sample cell. The infrared filter is used to minimize heating of the sample by the light source. After passing through the cell, the beam is reflected by a 45°

mirror upward through a matched pair of lenses to a long working distance optical microscope objective coupled to a Pulnix digital camera. The camera obtains images with 1392×1040 pixels and an overall resolution of about 1.7 μm/pixel. The gap between the sapphire windows is approximately 1 mm.

It is worth noting that the camera's field of view does not cover the entire system. If there are sinking or floating crystals, or if there is a slight temperature gradient in the cross, it is possible that what is observed in the camera's field of view might not be representative of the system as a whole. However, more often than not, what we observed was an exquisite choreographed dance of dissolving or growing crystals in concert with fluctuating temperature, pressure, and volume, thus indicating that the images are usually an excellent guide to what is happening in the bulk of the sample.

3. Experiments

3.1. Sample Preparation

The sample solution was made from reagent grade anhydrous sodium sulfate (thenardite) powder (Aldrich, 99.99%). The powder was heated above 200°C to drive off any remaining water, and then combined with sufficient deionized water to make a solution of 15.5 wt.% Na_2SO_4.

The phase diagram for Na_2SO_4 at atmospheric pressure is shown in Fig. 1. Besides ice, there are two solid phases at this concentration, $Na_2SO_4 \cdot 7H_2O$ (the heptahydrate) and $Na_2SO_4 \cdot 10H_2O$ (mirabilite). Although only the latter is stable, the heptahydrate is also often observed (Hamilton and Hall, 2008), particularly in the case of rapid solidification.

3.2. Results at 50 MPa

The results for a typical, though fairly simple, run at a pressure of 50 MPa are shown in Fig. 2 as a plot of transducer voltage (approximately proportional to the sample volume) *vs.* temperature.

After pressurizing to 50 MPa at a temperature high enough for the sample to be a homogeneous liquid (point a) we began cooling. After supercooling to 286 K (point b) a sharp increase in volume indicated rapid crystallization (point c); by further data analysis, including interpretation of the optical images, we deduced that this phase could only have been mirabilite. (The temperature is high enough that $Na_2SO_4 \cdot 7H_2O$ can be ruled out.) Although mirabilite is denser than the original solution, the remaining water-rich solution is less dense, leading to a slight overall increase in volume.

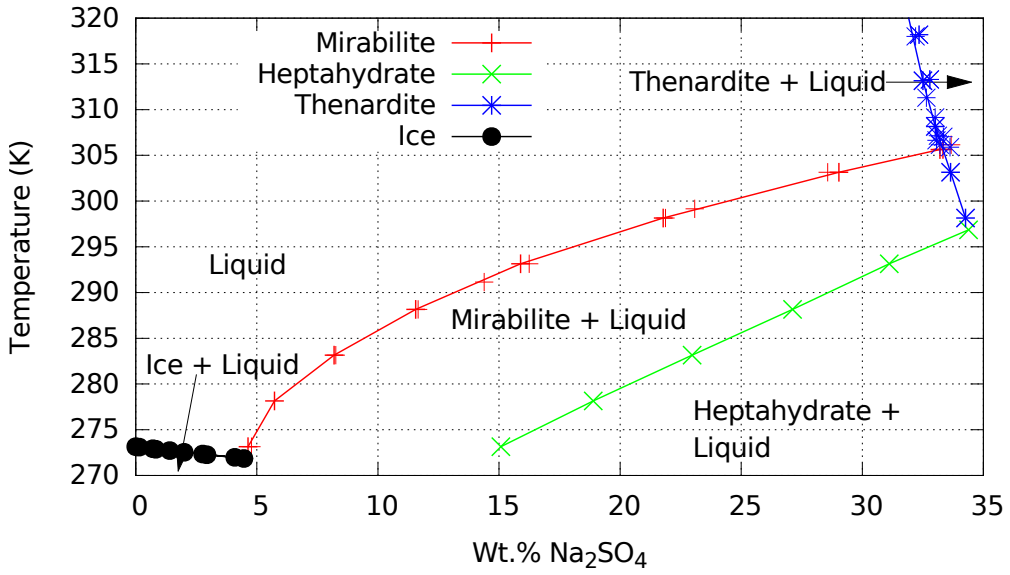

Figure 1: Phase diagram for Na_2SO_4, based on compilations by Eddy and Menzies (1940) and Wuite (1913).

This solid material continued to grow as we cooled the system to 255 K (point d). At that point, the remaining supercooled sample solidified rapidly to a much less dense, opaque mixture containing a significant mount of Ice Ih and, presumably, additional sulfate hydrate. Although the pure materials in this sample produce crystals that are inherently transparent, the multiple small grains in this sample bent and scattered the light so that the image became dark. Further cooling over the next 6 hours (to point e) produced no significant changes.

Upon warming, light began to filter through the sample almost immediately and the images revealed shifting structures that could be recrystallization or the early onset of melting. At about 250 K it became clear that the opaque material was dissolving and pieces could be seen floating upward. We were surprised to find liquid at such a low temperature. The likely explanation is that frozen material had blocked the connection between the pressure cell and the rest of the apparatus, including the pressure gauge and transducer. Further crystallization of low-density ice Ih in the cell could then have increased the pressure in the cell dramatically, but since the sample was

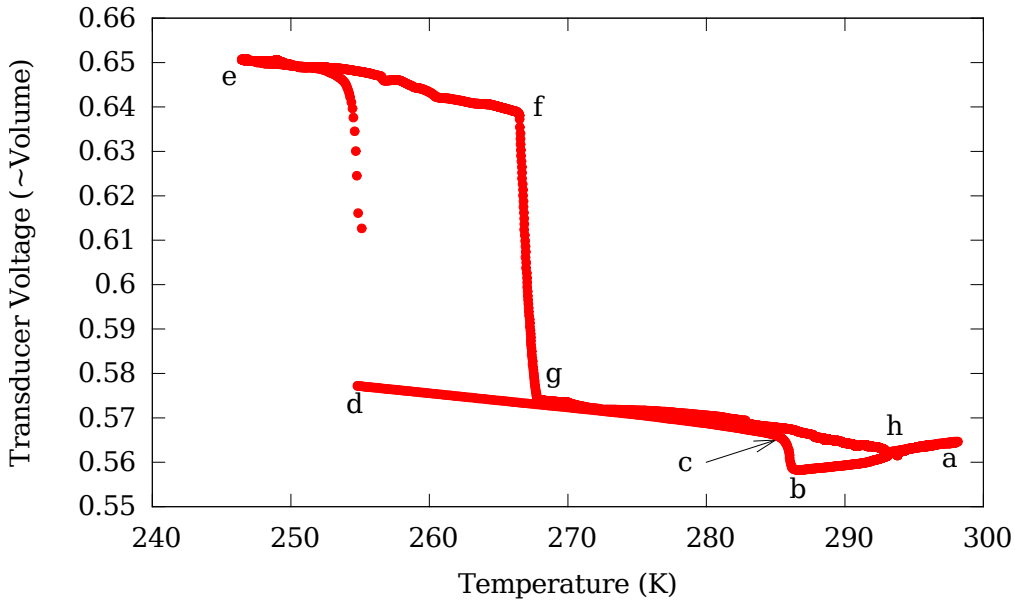

Figure 2: Plot of transducer voltage *vs.* Temperature for a run at a nominal pressure of 50 MPa. (The voltage changes approximately linearly with volume.) The lettered points are described in the text. Eutectic melting occurred near 267 K, though the temperature rose slightly as the pressure decreased.

frozen solid, the transducer did not reflect these changes between points (e) and (f) in Fig. 2.

This explanation is supported by runs on pure water, where we observed similar large increases in pressure when the system was locked up. For example, in one run with pure water, the system was frozen solid with the pressure gauge reading 5.24 MPa. As we warmed to a temperature of 257 K, however, we observed that the ice started to melt. From that temperature, we infer that the pressure inside the vessel had risen to about 163 MPa, far above the reading on the pressure gauge. However, while the system can become "locked up" when frozen solid, it must be emphasized that when warming is slow and melting becomes well advanced, the instrumental measurements reflect a well equilibrated system, and track pressure and volume changes with high precision.

With further warming, the original mirabilite crystals were soon revealed in the same form they had when they were suddenly obscured by the opaque material. The last of the opaque material disappeared from the image and

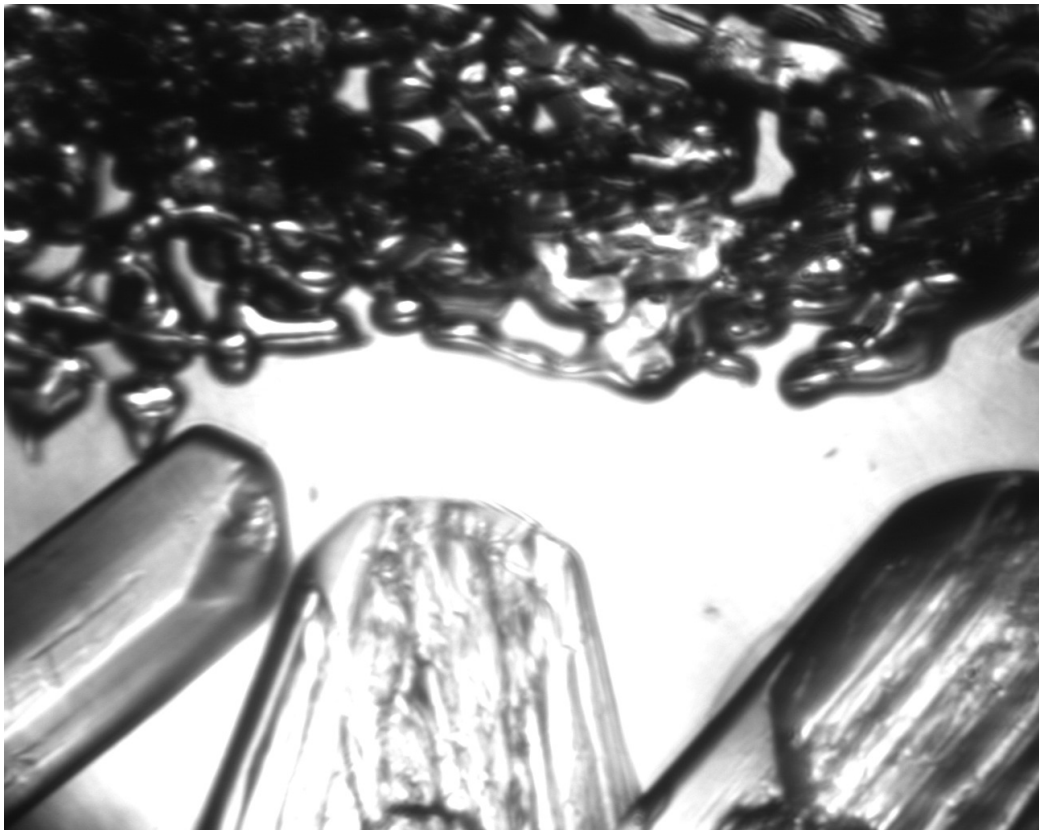

Figure 3: Ice Ih (top) and mirabilite (bottom) coexisting at 50 MPa. Gravity points downward. The image is about 2.4 mm across. The bright area in the center of the image is liquid. The melting ice crystals at this point are physically detached from each other and from the sides of the pressure vessel, and so the shrinking aggregation of buoyant ice crystals is freely floating upward, whereas the dense hydrate phase collapses downward as the crystalline trusswork melts and sinks. With the two solid phases plus liquid coexisting, and the spatial scale apparently being small compared to the solution's combined advective and diffusive mixing scale, the system is at the eutectic.

the mirabilite crystals could be observed to be dissolving well before point f was reached in Fig. 2. The rapid drop in voltage starting at point (f) indicated eutectic melting at 267 K. (The rapid drop also indicates that the system was no longer locked up, and that the pressure and voltage transducers accurately reflected the conditions in the sample.) An example image showing the coexistence of both ice Ih and mirabilite is shown in Fig. 3.

Continued warming along the mirabilite coexistence curve led to slow dis-

solution of the remaining crystals until point (h) was reached, corresponding to the liquidus temperature for this composition and pressure. A complete run typically took about 7 days.

3.3. Results at 250 MPa

The results for the same sample at a nominal pressure of 250 MPa are shown in Fig. 4. The run started (at point a) as a homogeneous liquid. We then started cooling.

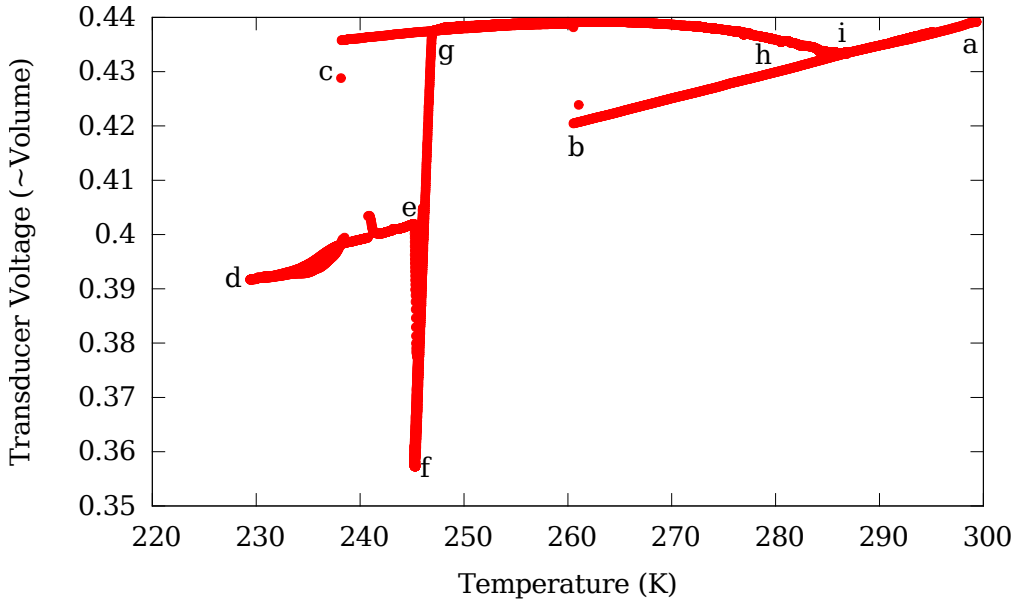

Figure 4: Plot of transducer voltage *vs.* Temperature for a run at a nominal pressure of 250 MPa. (The voltage changes approximately linearly with volume.) The lettered points are described in the text.

The trend of the liquid cooling curve from (a) to (b) involves thermal contraction of the liquid as it enters a region of supercooling with respect to the equilibrium liquidus solid phase, mirabilite. After supercooling to 260 K (point b), rapid crystallization led to a sharp increase in volume and a small increase in temperature due to the exothermic release of heat of crystallization; this heating effect is small (almost undiscernible in Fig. 4) because not only the sample but the surrounding capsule and steel must also be warmed in order for the thermometer to sense it.

The original growth was in the form of thin, plate-like crystals. These initial crystals are inferred to be mirabilite based on the topology of the phase diagram, the impossibility of any ice phase forming at this temperature and pressure (and surviving later in the experiment to a much higher temperature), and the form of the crystals. Following equilibration of the system with coexistence of one solid hydrate phase and the liquid, the crystals continued to grow slowly as we cooled the system to 238 K (toward point c), where the system was again supercooled, but this time metastable in that the expected ice III did not crystallize immediately as the system would require for equilibrium. At point (c) the system finally crystallized another solid, which we infer was ice III. This sudden episode of quench crystallization produced an opaque assemblage. Ice III crystallization produced a denser system (lower volume) both because the density of ice III is greater than the sodium sulfate solution, and because its crystallization pushed the liquid phase to a denser, more saline composition.

Further cooling to (d) produced no observable changes in the image because of the high opacity of the system. However, with quench crystallization of ice, enough of the sample (probably all of the remaining liquid) froze to block the inlet to the cross, hydraulic pressure equilibrium with the pressurizing fluid was apparently lost (as we commonly observed when quench solidification takes place), and the reduction in phase volume caused a rapid drop in pressure, thus reducing the compression of the sample without being detected by the pressure gauge or voltage transducer. These events in the region of point (d) are inferred, since we could not see what was happening, but are supported by our observations in numerous runs. Upon warming to point (e), incipient melting or softening of the sample near the melting point may have allowed pressure equilibrium with the pressurizing fluid to be reestablished, thus causing a surge in sample pressure and reduction in volume from (e) to (f). From (f) onward in Fig. 4, pressure equilibrium apparently existed in the semi-melted sample.

From (f) to (g), a reversible eutectic melting transition occurred near 246 K; as some solids, and especially the quenched ice crystals melted, sample opacity was reduced and the original mirabilite crystals re-emerged in the field of view. This transition was reversible. Upon re-cooling slightly, the voltage would drop and crystals could be observed regrowing in the window. After ice III was exhausted in the sample, further warming along the mirabilite/liquid coexistence curve (to point h) led to slow dissolution of the remaining crystals that were first observed at point (b).

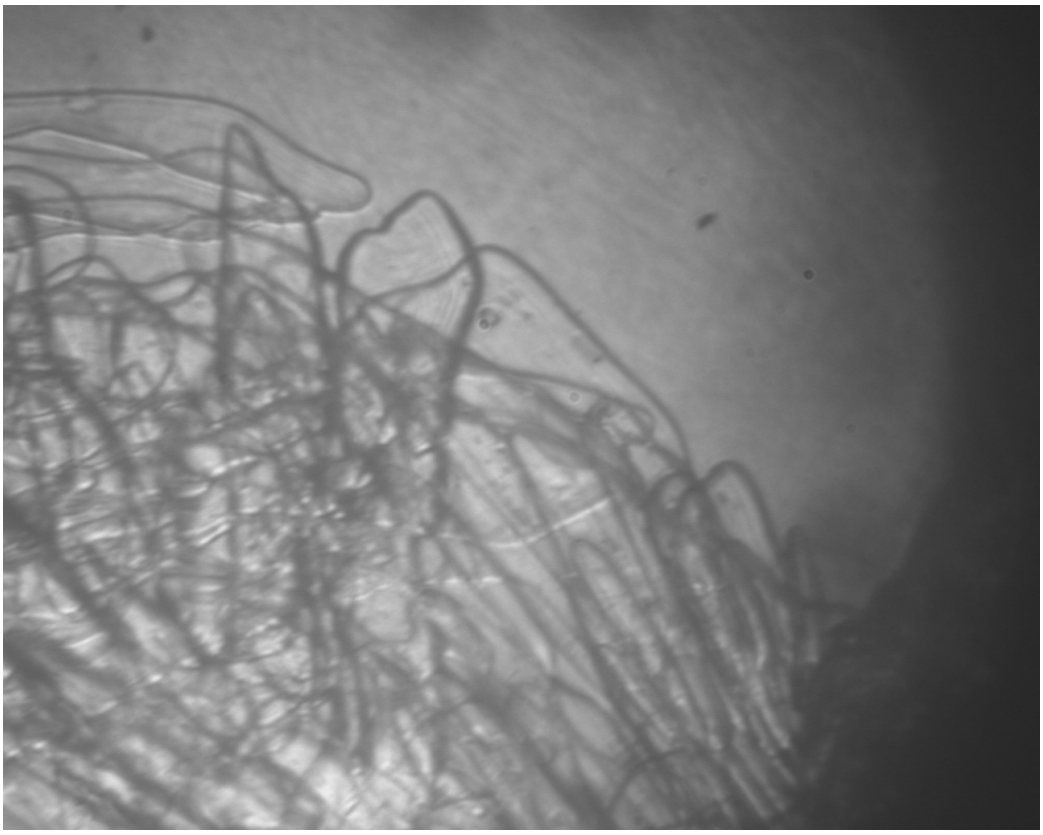

Figure 5: Crystals slowly dissolving at a pressure of 250 MPa and a temperature of 278 K, corresponding to point (h) in Fig. 4. The image is about 2.4 mm across. The light area in the top half of the image is liquid solution. The temperature is too high for the crystals to be anything but a hydrate phase. However, resorption has caused them to lose their diagnostic euhedral crystal forms; based on the topology of the phase diagram and the crystal forms observed earlier in the run, it is concluded that these crystals are mirabilite at a temperature just a bit colder than the liquidus (point i).

Fig. 5 shows the flat, nearly transparent crystals dissolving at point (h), where they have lost their initial euhedral nature. Warming continued until a discrete, well-defined liquidus was reached at (i). The distinct concave-down path taken between points (g) and (i) indicates that that the 250-MPa equivalent of the mirabilite liquidus shown in Fig. 1 is also strongly concave down in the segment between the eutectic and the liquidus for this 15.5 wt.% composition.

4. Results for the Eutectic Temperature and Pressure

In order to determine the eutectic temperature as a function of pressure, we considered only those points on reversible transitions where the volume was varying rapidly and the crystals were clearly either growing or dissolving in the window. For runs such as those in Figs. 2 and 4, those points were in a region between points (f) and (g).

The overall results are shown in Fig. 6. For comparison, we also show the melting temperatures for pure ice based on the curves reported by Wagner et al. (2011), and the ice phase boundaries based on the data tabulated by Dunaeva et al. (2010).

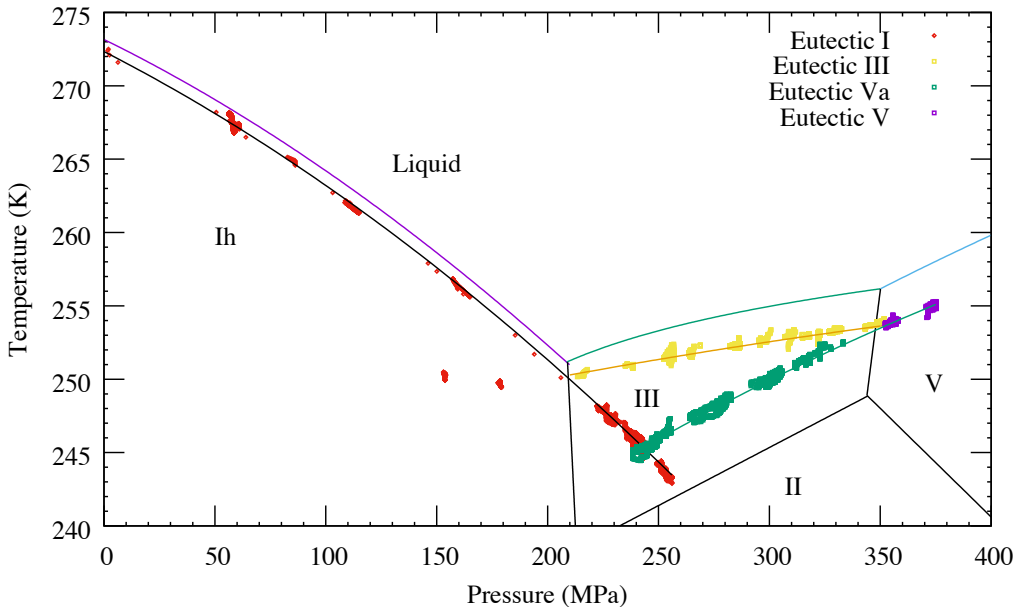

Figure 6: Results for all runs. Shown for comparison are the pure Ice Ih, Ice III, and Ice V melting curves from Wagner et al. (2011), and the phase boundaries for the different ice phases from Dunaeva et al. (2010). The solid lines through the data are fits described in the text.

For the Ice melting curves, we use the functions recommended by Wagner et al. (2011):

$$\frac{p}{p_0} = 1 + \sum_{1}^{3} a_i \left(1 - \left(\frac{T}{T_0} \right)^{b_i} \right) \tag{1}$$

where the numerical values of the parameters are given in Wagner et al. (2011).

To minimize fitting artifacts, we initially used the same functional form for our data. However, our data do not cover a wide enough range of temperatures to constrain the parameters, particularly in the Ice III regime, especially since the the values for p_0, and T_0 are not independently known. As a result, the typical uncertainties in the fit parameters a_i and b_i, were often larger than the fit parameters themselves.

We also considered the melting curve equation proposed by Kechin (1995), based on a modification of the Simon-Glatzel equation (Simon and Glatzel, 1929).

$$\frac{T}{T_0} = \left(1 + \frac{\Delta p}{a_1}\right)^{a_2} \exp\left(-a_3 \Delta p\right) \tag{2}$$

where $\Delta p = p - p_0$. This is similar to including a single term from Eq. 1, but with an additional exponential decay term a_3. However, that term did not significantly improve the quality of the fit, and the values for a_3 were consistent with zero. We also considered other forms sometimes used for the melting of pure substances, such as that recommended by Yi-Jing et al. (1982), but they either did not fit as well over the full range of the data, or required more parameters that were typically poorly-constrained.

The best description of the data was ultimately obtained with simple polynomial fits of the form

$$T = a_0 + a_1(p - p_0) + a_2(p - p_0)^2 \tag{3}$$

where p_0 was arbitrarily fixed to correspond with the relevant data range.

4.1. Pressure dependence of the Eutectic Temperature: Ice Ih Regime

In the Ice Ih regime, the best-fit values for Eq. 3 are given in Table 1.

p_0	0 MPa
a_0	272.33 ± 0.02 K
a_1	-0.0775 ± 0.0004 K/MPa
a_2	$-(1.38 \pm 0.01) \times 10^{-4}$ K/MPa^2

Table 1: Fit to Eq. 3 for eutectic temperature in the Ice-Ih regime

In two runs, near 150 and 175 MPa, we observed anomalously low eutectic temperatures. We were not able to repeat them at other pressures, but include them in the figure for completeness.

Although Ice Ih is stable only up to 209 MPa, we were able to observe higher pressure metastable states by slowly raising the pressure from below 209 MPa while simultaneously lowering the temperature. Above about 250 MPa, however, the system would quickly and irreversibly change to a higher-density ice phase.

4.2. Pressure dependence of the Eutectic Temperature: Ice III Regime

In the Ice III regime, we observed two distinct transitions. In most runs, we observed a modest freezing point depression that increased slightly with pressure. These results are labeled as "Eutectic III" in Fig. 6. However, in a number of other cases, the eutectic temperature was significantly lower. These are labeled as "Eutectic Va" in Fig. 6; an example run was shown in Fig. 4.

Unfortunately, the images in these cases do not show distinct crystal forms that enable us clearly identify the phases involved. Both solids are more dense than the liquid solution. The state labeled Va had a higher density than III, but we were not able to measure absolute densities of solids with this apparatus. Both transitions were several degrees above the Ice II equilibrium curve. The lower-temperature data do follow an extension of the Ice V regime curve, consistent with the formation of metastable Ice V, as suggested by Evans (1967), and are included in the Ice V regime fits described below.

For the III phase, the best-fit values for Eq. 3 are given in Table 2.

p_0	209.0 MPa
a_0	250.26 ± 0.01 K
a_1	0.0276 ± 0.0004 K/MPa
a_2	$-(2.7 \pm 0.2) \times 10^{-5}$ K/MPa^2

Table 2: Fit to Eq. 3 for the eutectic temperature in the Ice-III regime.

4.3. Pressure dependence of the Eutectic Temperature: Ice V Regime

The III and Va curves converge as pressure increases and the fitted lines intersect quite close to the Ice III-V boundary. Above around 350 MPa, we only ever observed a single phase.

The best-fit values for Eq. 3 for the Ice V regime are given in Table. 3:

p_0	350.0 MPa
a_0	253.480 ± 0.004 K
a_1	0.0667 ± 0.0001 K/MPa
a_2	$-(8.9 \pm 0.1) \times 10^{-5}$ K/MPa^2

Table 3: Fit to Eq. 3 for the eutectic temperature in the Ice V regime, including the metastable "Va" points in Fig.6 above.

5. Discussion

We have determined the eutectic point for aqueous sodium sulfate solutions for pressures ranging from 0.1 to 375 MPa. The freezing point depression due to the presence of the Na_2SO_4 was generally rather small over the full range of pressures explored in this work. In the Ice-Ih regime, it was typically about 1.0 K. In the Ice-III regime, the depression increased with pressure to roughly 2.5 K. In the Ice-V regime, it was slightly less than 3 K; we were not able to obtain data over 375 MPa with this apparatus, so we were not able to determine any clear trend for Ice-V. In all cases, these phase changes were accompanied by significant changes in volume.

Even within our small sample, we observed a number of deviations from thermodynamic equilibrium. The sodium sulfate system can be supercooled significantly—supercoolings of more than 20 K, as seen in Fig. 4, were readily obtained. We also observed long-lasting metastable states within the Ice-III region. In addition, we found that the system exhibits very sluggish dynamics as it relaxes towards equilibrium. For Fig. 4, for example, the whole run lasted about 1 week, and the warming towards the liquidus proceeded at a rate of approximately 0.16 K/hour. Accordingly, dynamic processes that operate on shorter time scales or across larger length scales should not necessarily be assumed to be occurring in thermodynamic equilibrium.

Acknowledgments

This research was partially supported by Grant # NAGD5-12829 from the NASA Cosmochemistry program.

Brown, M. E., Hand, K. P., Apr. 2013. Salts and radiation products on the surface of Europa. Astron. J. 145 (4), 110.

Carlson, R., Anderson, M., Mehlman, R., Johnson, R., 2005. Distribution of hydrate on Europa: Further evidence for sulfuric acid hydrate. Icarus 177 (2), 461–471.

Carlson, R., Smythe, W., Baines, K., Barbinis, E., Becker, K., Burns, R., Calcutt, S., Calvin, W., Clark, R., Danielson, G., Davies, A., Drossart, P., Encrenaz, T., Fanale, F., Granahan, J., Hansen, G., Herrera, P., Hibbitts, C., Hui, J., Irwin, P., Johnson, T., Kamp, L., Kieffer, H., Leader, F., Lellouch, E., LopesGautier, R., Matson, D., McCord, T., Mehlman, R., Ocampo, A., Orton, G., RoosSerote, M., Segura, M., Shirley, J., Soderblom, L., Stevenson, A., Taylor, F., Torson, J., Weir, A., Weissman, P., 1996. Near-infrared spectroscopy and spectral mapping of Jupiter and the Galilean satellites: Results from Galileo's initial orbit. Science 274 (5286), 385–388.

Dalton, J., Prieto-Ballesteros, O., Kargel, J., Jamieson, C., Jolivet, J., Quinn, R., 2005. Spectral comparison of heavily hydrated salts with disrupted terrains on Europa. Icarus 177 (2), 472–490.

Dougherty, A. J., Bartholet, Z. T., Chumsky, R. J., Delano, K. C., Huang, X., Morris, D. K., Dec. 2018. The Liquidus Temperature for Methanol-Water Mixtures at High Pressure and Low Temperature, With Application to Titan. J. Geophys. Res.-Planets 123 (12), 3080–3087.

Dunaeva, A. N., Antsyshkin, D. V., Kuskov, O. L., Jun. 2010. Phase diagram of H(2)O: Thermodynamic functions of the phase transitions of high-pressure ices. Sol Syst. Res. 44 (3), 202–222.

Durham, W., Stern, L., Kubo, T., Kirby, S., 2005. Flow strength of highly hydrated Mg- and Na-sulfate hydrate salts, pure and in mixtures with water ice, with application to Europa. J. Geophys. Res. 110 (E12).

Eddy, R. D., Menzies, A. W. C., 1940. The solubilities of certain inorganic compounds in ordinary water and in deuterium water. J. Phys. Chem. 44, 207–235.

Evans, L. F., 1967. Selective nucleation of high-pressure ices. J. Appl. Phys. 38 (12), 4930–4932.

Feldman, W., Mellon, M., Maurice, S., Prettyman, T., Carey, J., Vaniman, D., Bish, D., Fialips, C., Chipera, S., Kargel, J., Elphic, R., Funsten, H.,

Lawrence, D., Tokar, R., 2004. Hydrated states of MgSO4 at equatorial latitudes on Mars. Geophys. Res. Lett. 31 (16).

Fialips, C. I., Carey, J. W., Vaniman, D. T., Bish, D. L., Feldman, W. C., Mellon, M. T., 2005. Hydration state of zeolites, clays, and hydrated salts under present-day Martian surface conditions: Can hydrous minerals account for Mars Odyssey observations of near-equatorial water-equivalent hydrogen? Icarus 178 (1), 74–83.

Fischer, P. D., Brown, M. E., Hand, K. P., Nov. 2015. Spatially resolved spectroscopy of europa: the distinct spectrum of large-scale chaos. Astron. J. 150 (5), 164.

Flatt, R., 2002. Salt damage in porous materials: how high supersaturations are generated. J. Cryst. Growth 242 (3-4), 435–454.

Flatt, R. J., Caruso, F., Sanchez, A. M. A., Scherer, G. W., Sep. 2014. Chemomechanics of salt damage in stone. Nature Communications 5, 4823.

Fox-Powell, M. G., Osinski, G. R., Applin, D., Stromberg, J. M., Gazquez, F., Cloutis, E., Allender, E., Cousins, C. R., Jun. 2019. Natural Analogue Constraints on Europa's Non-ice Surface Material. Geophys. Res. Lett. 46 (11), 5759–5767.

Grundy, W. M., Buratti, B. J., Cheng, A. F., Emery, J. P., Lunsford, A., McKinnon, W. B., Moore, J. M., Newman, S. F., Olkin, C. B., Reuter, D. C., Schenk, P. M., Spencer, J. R., Stern, S. A., Throop, H. B., Weaver, H. A., Team, N. H., Oct. 2007. New Horizons mapping of Europa and Ganymede. Science 318 (5848), 234–237.

Hamilton, A., Hall, C., 2008. Sodium sulfate heptahydrate: a synchrotron energy-dispersive diffraction study of an elusive metastable hydrated salt. J. Anal. Atomic Spectroscopy 23.

Hand, K., Carlson, R., 2015. Europa's surface color suggests an ocean rich with sodium chloride. Geophys. Res. Lett. 42 (9), 3174.

Haynes, H., 2005. ASTM C 88 Test on soundness of aggregate using sodium sulfate or magnesium sulfate: A study of the mechanisms of damage. J. ASTM Intl. 2, 17.

Hogenboom, D., Kargel, J., Consolmagno, G., Holden, T., Lee, L., Buyyounouski, M., 1997. The ammonia-water system and the chemical differentiation of icy satellites. Icarus 128 (1), 171–180.

Hogenboom, D., Kargel, J., Ganasan, J., Lee, L., 1995. Magnesium sulfate-water to 400 MPa using a novel piezometer - densities, phase-equilibria, and planetological implications. Icarus 115 (2), 258–277.

Kargel, J., Kaye, J., Head, J., Marion, G., Sassen, R., Crowley, J., Ballesteros, O., Grant, S., Hogenboom, D., 2000. Europa's crust and ocean: Origin, composition, and the prospects for life. Icarus 148 (1), 226–265.

Kechin, V. V., Jan. 1995. Thermodynamically based melting-curve equation. J. Phys.: Condens. Matter 7 (3), 531–535.

Ligier, N., Poulet, F., Carter, J., Brunetto, R., Gourgeot, F., Jun. 2016. Vlt/sinfoni observations of Europa: New insights into the surface composition. Astron. J. 151 (6), 163.

McCarthy, C., Cooper, R. F., Kirby, S. H., Durham, W. B., 2006. Ice/hydrate eutectics: The implications of microstructure and rheology on a multiphase Europan crust. In: LPSC XXXVII.

McCord, T., Hansen, G., Fanale, F., Carlson, R., Matson, D., Johnson, T., Smythe, W., Crowley, J., Martin, P., Ocampo, A., Hibbitts, C., Granahan, J., 1998. Salts an Europa's surface detected by Galileo's near infrared mapping spectrometer. Science 280 (5367), 1242–1245.

McCord, T., Hansen, G., Matson, D., Johnson, T., Crowley, J., Fanale, F., Carlson, R., Smythe, W., Martin, P., Hibbitts, C., Granahan, J., Ocampo, A., 1999. Hydrated salt minerals on Europa's surface from the Galileo near-infrared mapping spectrometer (NIMS) investigation. J. Geophys. Res. 104 (E5), 11827–11851.

McCord, T. B., Hansen, G. B., Combe, J.-P., Hayne, P., Oct. 2010. Hydrated minerals on Europa's surface: An improved look from the Galileo NIMS investigation. Icarus 209 (2), 639–650.

McKinnon, W., Zolensky, M., 2003. Sulfate content of Europa's ocean and shell: Evolutionary considerations and some geological and astrobiological implications. Astrobiology 3 (4), 879–897.

McMahon, D. J., Sandberg, P., Folliard, K., Mehta, P. K., 1992. Deterioration mechanisms of sodium sulfate. In: 7th International Conference on the Deterioration and Preservation of Stone, Lisbon, Portugal. Vol. June. pp. 705–714.

Neveu, M., Desch, S. J., Castillo-Rogez, J. C., Sep. 2017. Aqueous geochemistry in icy world interiors: Equilibrium fluid, rock, and gas compositions, and fate of antifreezes and radionuclides. Geochimica Et Cosmochimica Acta 212, 324–371.

Nimmo, F., Pappalardo, R. T., Aug. 2016. Ocean worlds in the outer solar system. J. Geophys. Res. Planets 121 (8), 1378–1399.

Orlando, T., McCord, T., Grieves, G., 2005. The chemical nature of Europa surface material and the relation to a subsurface ocean. Icarus 177 (2), 528–533.

Prockter, L. M., Lopes, R. M. C., Giese, B., Jaumann, R., Lorenz, R. D., Pappalardo, R. T., Patterson, G. W., Thomas, P. C., Turtle, E. P., Wagner, R. J., Jun. 2010. Characteristics of icy surfaces. Space Sci. Rev. 153 (1-4), 63–111.

Prockter, L. M., Shirley, J. H., Dalton,James B.,, I., Kamp, L., Mar. 15 2017. Surface composition of pull-apart bands in Argadnel Regio, Europa: Evidence of localized cryovolcanic resurfacing during basin formation. Icarus 285, 27–42.

Rijniers, L. A., Huinink, H. P., Pel, L., Kopinga, K., 2005. Experimental evidence of crystallization pressure inside porous media. Phys. Rev. Lett. 94, 075503.

Roth, L., Saur, J., Retherford, K. D., Strobel, D. F., Feldman, P. D., McGrath, M. A., Nimmo, F., Jan. 10 2014. Transient water vapor at Europa's south pole. Science 343 (6167), 171–174.

Scherer, G. W., 2004. Stress from crystallization of salt. Cement and Concrete Research 34 (9), 1613–1624.

Schmidt, B. E., Blankenship, D. D., Patterson, G. W., Schenk, P. M., Nov. 24 2011. Active formation of "chaos terrain" over shallow subsurface water on Europa. Nature 479 (7374), 502–505.

Shirley, J. H., Dalton,James B.,, I., Prockter, L. M., Kamp, L. W., Nov. 2010. Europa's ridged plains and smooth low albedo plains: Distinctive compositions and compositional gradients at the leading side-trailing side boundary. Icarus 210 (1), 358–384.

Simon, F., Glatzel, G., 1929. Bemerkungen zur schmelzdruckkurve. Z. Anorg. Allg. Chem. 178 (1), 309–316.

Soderlund, K. M., Schmidt, B. E., Wicht, J., Blankenship, D. D., Jan. 2014. Ocean-driven heating of Europa's icy shell at low latitudes. Nature Geoscience 7 (1), 16–19.

Sparks, W. B., Schmidt, B. E., McGrath, M. A., Hand, K. P., Spencer, J. R., Cracraft, M., Deustua, S. E., Apr. 20 2017. Active cryovolcanism on Europa? Astrophys. J., Lett. 839 (2), L18.

Spaun, N., Head, J., 2001. A model of Europa's crustal structure: Recent Galileo results and implications for an ocean. J. Geophys. Res. 106 (E4), 7567–7575.

Szynkiewicz, A., Borrok, D. M., Vaniman, D. T., May 1 2014. Efflorescence as a source of hydrated sulfate minerals in valley settings on Mars. Earth Planet. Sci. Lett. 393, 14–25.

Tanaka, Y., Hada, S., Makita, T., Moritoki, M., 1992. Effect of pressure on the solid-liquid phase-equilibria in (water + sodium-sulfate) system. Fluid Phase Equilib. 76, 163–173.

Trumbo, S. K., Brown, M. E., Hand, K. P., Jun. 2019. Sodium chloride on the surface of Europa. Sci. Adv. 5 (6), eaaw7123.

Vance, S. D., Barge, L. M., Cardoso, S. S. S., Cartwright, J. H. E., May 2019. Self-Assembling Ice Membranes on Europa: Brinicle Properties, Field Examples, and Possible Energetic Systems in Icy Ocean Worlds. Astrobiology 19 (5), 685–695.

Vaniman, D., Bish, D., Chipera, S., Fialips, C., Carey, J., Feldman, W., 2004. Magnesium sulphate salts and the history of water on Mars. Nature 431 (7009), 663–665.

Wagner, W., Riethmann, T., Feistel, R., Harvey, A. H., Dec. 2011. New Equations for the Sublimation Pressure and Melting Pressure of H(2)O Ice Ih. J. Phys. Chem. Ref. Data 40 (4).

Wang, A., Feldman, W. C., Mellon, M. T., Zheng, M., Sep.-Oct. 2013 2013. The preservation of subsurface sulfates with mid-to-high degree of hydration in equatorial regions on Mars. Icarus 226 (1), 980–991.

Wuite, J. P., 1913. Z. Physik. Chem. 86, 349–382.

Yi-Jing, D., Tsu-Tung, Y., Li-Rong, C., 1982. On the equation for the pressure-dependence of melting temperature. J. Phys. D: Appl. Phys. 15 (2), 263–265.

Zolotov, M. Y., Krieg, M. L., Shock, E. L., McKinnon, W. B., 2006. Chemistry of a primordial ocean on Europa. In: LPSC XXXVII.